IOPscience iopscience.iop.org

Home Search Collections Journals About Contact us My IOPscience

A ball-bearing structured triboelectric nanogenerator for nondestructive damage and rotating speed measurement

This content has been downloaded from IOPscience. Please scroll down to see the full text.

2016 Nanotechnology 27 085401

(http://iopscience.iop.org/0957-4484/27/8/085401)

View the table of contents for this issue, or go to the journal homepage for more

Download details:

IP Address: 143.215.239.150
This content was downloaded on 25/01/2016 at 15:26

Please note that terms and conditions apply.

IOP Publishing Nanotechnology
Nanotechnology 27 (2016) 085401 (9pp) doi:10.1088/0957-4484/27/8/085401

A ball-bearing structured triboelectric nanogenerator for nondestructive damage and rotating speed measurement

Xiao Hui Li[1,3], Chang Bao Han[1,3], Tao Jiang[1], Chi Zhang[1] and Zhong Lin Wang[1,2]

[1] Beijing Institute of Nanoenergy and Nanosystems, Chinese Academy of Sciences, Beijing, 100083, People's Republic of China
[2] School of Material Science and Engineering, Georgia Institute of Technology, Atlanta, GA 30332, USA

E-mail: zlwang@gatech.edu

Received 20 August 2015, revised 29 November 2015
Accepted for publication 21 December 2015
Published 25 January 2016

Abstract

A ball-bearing structure based triboelectric nanogenerator (B-TENG) with interdigitative-electrodes was developed that can not only collect energy from rotational kinetic energy, but also serve as a self-powered and multifunctional sensor. The B-TENG relies on the rolling electrification between PTFE balls on Cu interdigitative-electrodes, which delivers an open-circuit voltage of ~40 V and a short-circuit current of ~1.2 μA at a rotating speed of 300 rpm for 4 mm PTFE balls. Using the output signals of B-TENG, a nondestructive detection for the damage of PTFE balls was realized without demounting the bearing. Besides, based on the periodic signals produced from B-TENG, the rotation speed of ball-bearing can be obtained according to the time difference between several cycles.

S Online supplementary data available from stacks.iop.org/NANO/27/085401/mmedia

Keywords: triboelectric nanogenerator, self-powered, rotating speed sensor, damage sensor

(Some figures may appear in colour only in the online journal)

Introduction

Nondestructive detection, which is able to inspect certain internal structure damage by means of sound [1], light [2], magnetic [3], and electrical [4] properties without cutting the tested object, is an essential technology in industrials applications, such as biological cells detection [5], chemical substances testing [6], aircraft structural flaws inspection [7]. For bearing defects, nondestructive detection on the basis of electric effects is a common technique for the inspection of bearing failures [8]. Recently, triboelectric nanogenerator (TENG) [9–12], which can effectively convert different types of mechanical energy from ambient environment into electricity, has been successfully explored to fabricate various types of self-powered systems, including artificial intelligence systems [13, 14], biomedical monitoring [15, 16], and wireless networks [17, 18], etc. Moreover, the output signals of TENG can make a quick respond with variation of the testing environment, such as vibration frequency [19, 20], velocity [21, 22], and rotating angle [23].

Here, for the first time, we propose a new application of TENG in the nondestructive damage detection fields. A ball-bearing structure and interdigitative-electrodes based TENG (B-TENG) was fabricated to establish a self-powered damage measurement sensor, as well as a rotating speed sensor. Based on a cyclic contact/separation between the PTFE balls and Cu interdigitative-electrodes, the B-TENG delivers an open-circuit voltage (V_{OC}) of ~40 V and a short-circuit current (I_{SC}) of ~1.2 μA at a rotating speed of 300 rpm when PTFE balls are 4 mm in diameter. According to the structure of B-TENG, rotation speeds were calculated by analyzing the output cyclic signals. Furthermore, certain damages on the bearing balls can be detected in real-time without open/cut the whole

[3] These authors contributed equally to this work.

 © 2016 IOP Publishing Ltd Printed in the UK

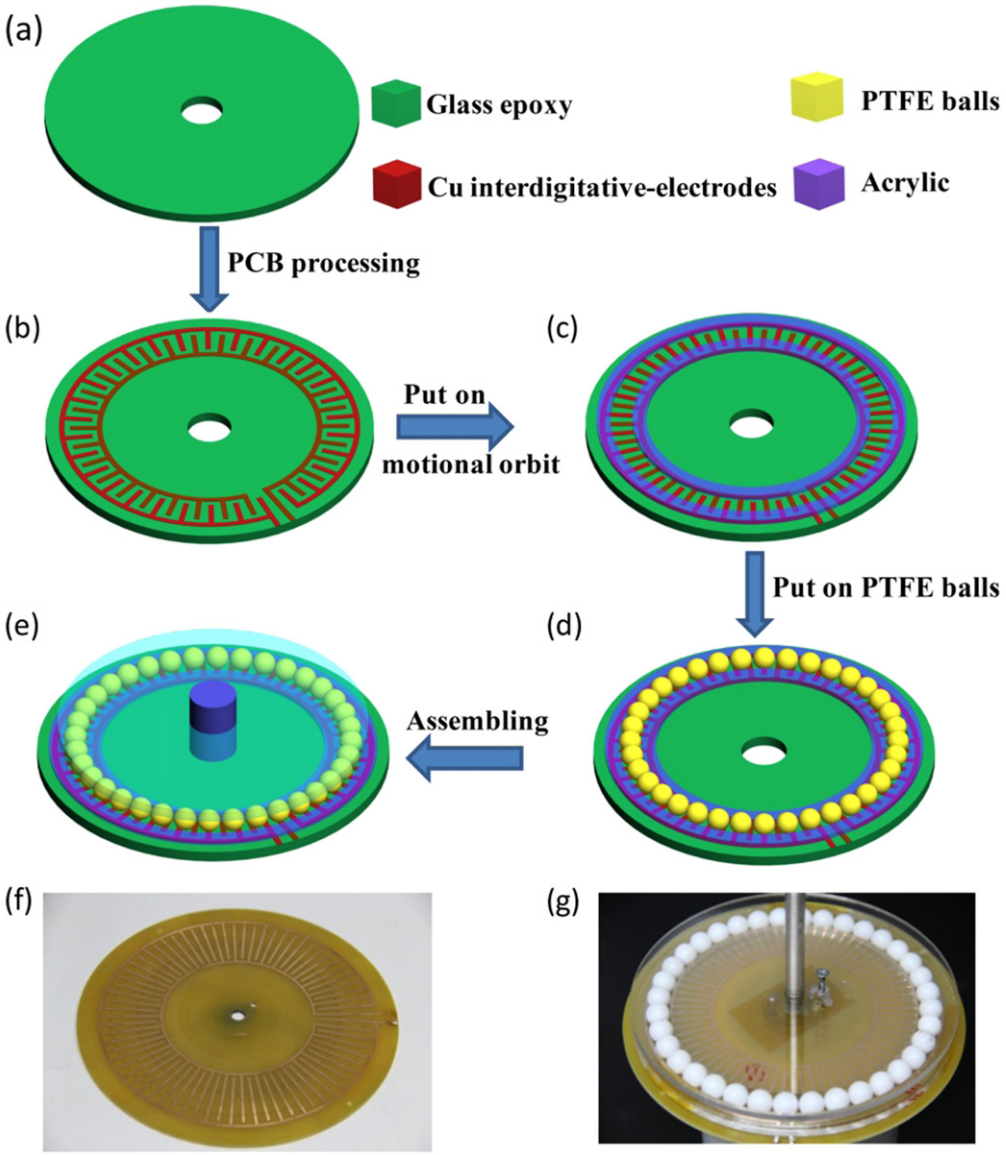

Figure 1. Schematic illustration of the fabrication process of the B-TENG. (a), (b) The interdigitative-electrodes are fabricated by the PCB technology. (c)–(e) The assembling of final B-TENG. (f) The photograph of Cu interdigitative-electrodes. (g) The photograph of an as-fabricated B-TENG after assembling.

bearing structure. This work presents a multi-functional self-powered system, and the fabricated B-TENG has a wide-spread application prospect in self-powered sensors, industrial inspection, and energy harvesting.

Experimental section

The Cu interdigitative-electrodes were first printed on the glass epoxy by printed circuit board (PCB) technology. Then, an acrylic sheet was cut into the ring shape by laser carving machine (PLS6.75, universal, USA). The two acrylic rings, outer ring and inner ring, were pasted on the disk in the next step, serving as the motional orbit of the PTFE balls. After that, a certain number of balls were put on the disk, and finally, another top sheet made of acrylic was put on the disk to finish the assembling process.

The output short-circuit current and open-circuit signals voltage were measured by Standford low-noise current pre-amplifier (SR570, Keithley, USA) and an oscilloscope (DSOX2014A, Agilent, USA), respectively. In addition, an electric rotating axis was applied to the B-TENG to make the PTFE balls roll around its orbit.

3D models were built based on the finite element method (FEM), and the input parameters used for this study are as follows: the inner diameter of orbit is 5.4 cm; the outer diameter of orbit is 7.4 cm; the diameter of PTFE ball is 1 cm; the number of PTFE balls is 20; the central angle between the adjacent electrodes is 9°; the thickness of Cu electrodes is 10 μm. In the FEM simulations, we used the 'electrostatics' module of COMSOL to calculate the electric potential

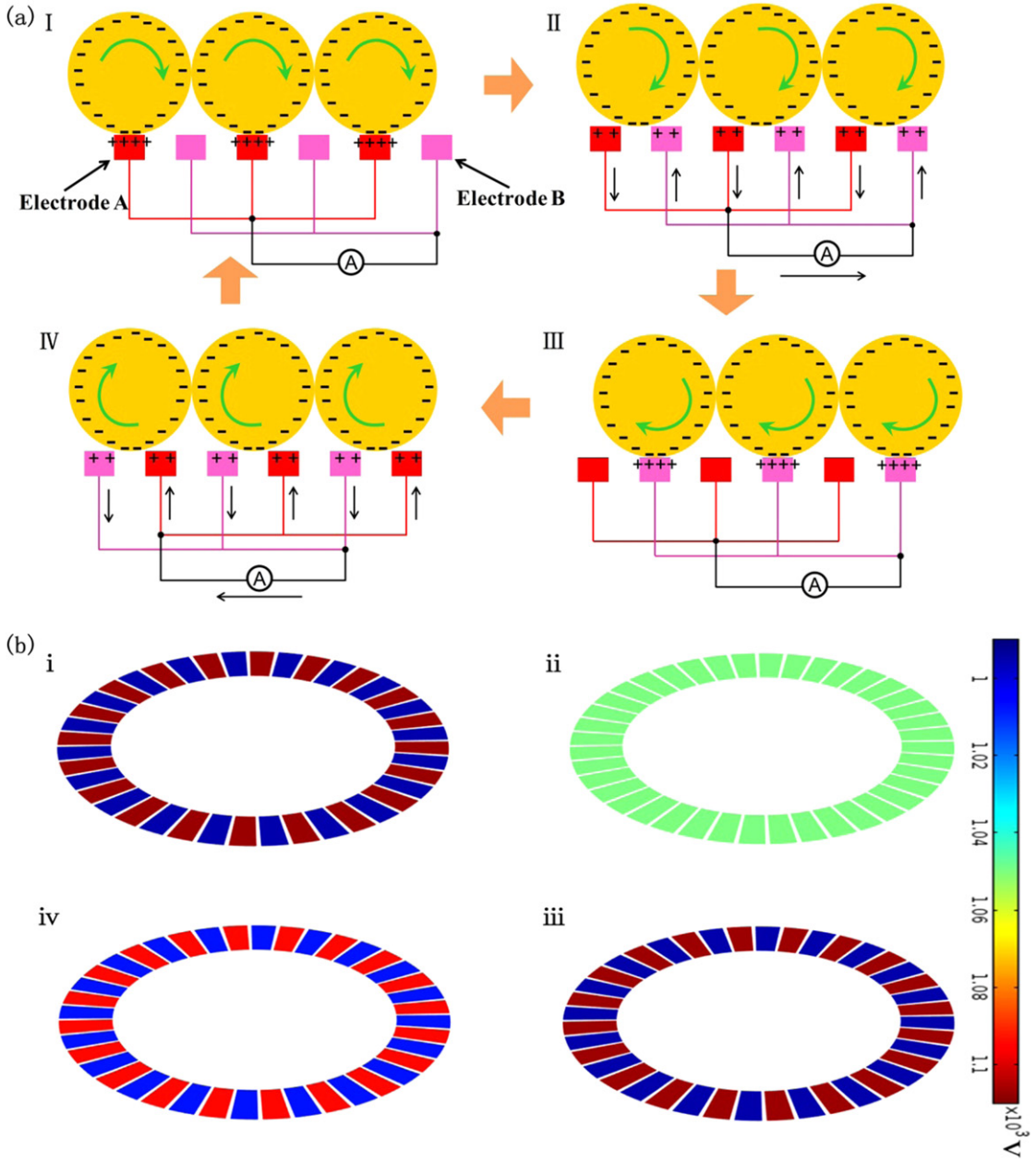

Figure 2. (a) Schematic diagrams of the working principle of the B-TENG in a complete cycle. (b) The potential distribution between the interdigitative-electrodes calculated by COMSOL in a complete cycle, (I) initial stage; (II) T/4 stage; (III) T/2 stage; (IV) 5T/8 stage.

distribution through the 'stationary' study. When we provided the boundary conditions, such as the surface charge density ($-30\ \mu C\ m^{-2}$), floating potential, ground, after the calculation, the potential and field information can be obtained and picked up in the 'results' section. First, we constructed the 3D model of TENG in the 'geometry' section through different shapes. Then in the 'materials' section, we set the property of the plate metal materials and spherical dielectric materials. The relative permittivity of dielectrics was set to be 2.0 to correspond to the PTFE materials. Next, the boundary conditions were chosen and the mesh was divided based on specific rules. Finally, we started to implement the computation in the 'study' section.

Results and discussion

The fabrication process of B-TENG is depicted in figures 1(a)–(e). The whole process starts from the fabrication of Cu interdigitative-electrodes through the mature PCB technology [24]. Then an appropriate motional orbit made up of acrylic is designed and fixed on the planar disk to make sure that those PTFE balls closely contact with each other. After that, a certain number of PTFE balls are put on the disk, and then a spindle and a top acrylic sheet are assembled with it, thus, a ball-bearing structure and interdigitative-electrodes based TENG was fabricated. The photographs of Cu electrodes after PCB processing and the final B-TENG were shown in figures 1(f) and (g), respectively.

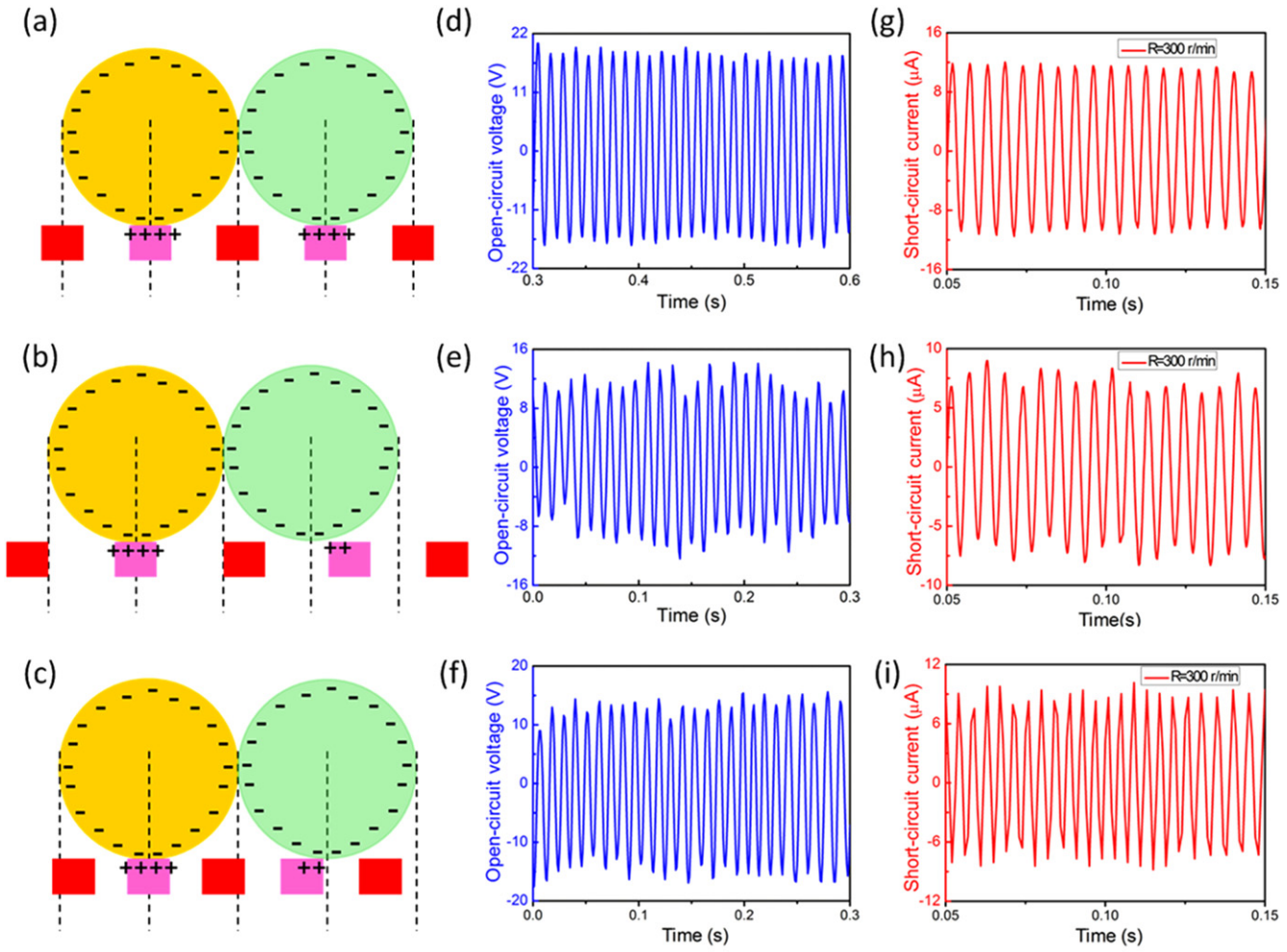

Figure 3. Electrical output characterization of the B-TENG with the balls of 4 mm in diameter. (a), (b), (c) Schematic diagram when $M = 2N$, $M < 2N$, and $M > 2N$, respectively. (d), (e), (f) and (g), (h), (i) are the corresponding V_{OC} and I_{SC} ofB-TENG, respectively.

The working principle of the B-TENG is demonstrated in figure 2(a). Here, we specify that PTFE balls contact closely with each other, and those balls are all aligned with the bottom electrode A and B, which represent a pair of interdigitative-electrodes. At the original stage I, we suppose that PTFE balls contact closely with electrode A. Since PTFE is more triboelectrically negative than Cu, it is prone to get negative charges evenly-distributed on the surface, leaving net positive charges on the Cu electrodes. The rolling of charged PTFE balls will induce charge flow from electrode B to electrode A through the external circuit until another electrostatic equilibrium is reached at the stage III. When the balls go on rolling along the orbit, electrons move back from electrode A to electrode B until reaching stage I again, and thus an alternating current (AC) is generated. The design of interdigitative-electrodes facilitates the periodic charge separation for electricity generation during the continuous rotating.

The electric potential distribution in the B-TENG and the charge transfer between the two electrodes can be verified though numerical simulation using COMSOL (figure 2(b)). The potential distributions on the interdigitative-electrodes under the open-circuit condition are shown at different stages in figure 2(b). From the full cycle result, at the initial stage, electrode A obtains the maximum voltage while electrode B gets the minimum one, resulting in the maximum output V_{OC} in the external circuit. With the rolling of PTFE balls caused by the rotating of rotator, the potential difference will then decrease to zero when PTFE balls move from initial stage to $T/4$ stage. Then, the maximum negative potential difference is generated when the PTFE balls contact closely with electrode B (at $T/2$ stage). Reversely, the potential difference increases from $T/2$ to T. The change of potential difference between the electrodes caused by periodic charge separation drives the current flowing through the external circuit during the rotating.

Figure 3 illustrates the electrical output of a B-TENG with the PTFE balls of 4 mm in diameter when those balls roll along three different orbits. For PTFE balls with a certain diameter, there is only one proper rolling orbit where the B-TENG is able to produce the maximum I_{SC} and V_{OC}. Such a proper orbit must satisfy the following conditions simultaneously: (1) all of the PTFE balls intimately contact with each other in the orbit; (2) PTFE balls should be matched with the interdigitative-electrodes (fully contact with electrodes A or electrodes B) in the initial stage, which will ensure the

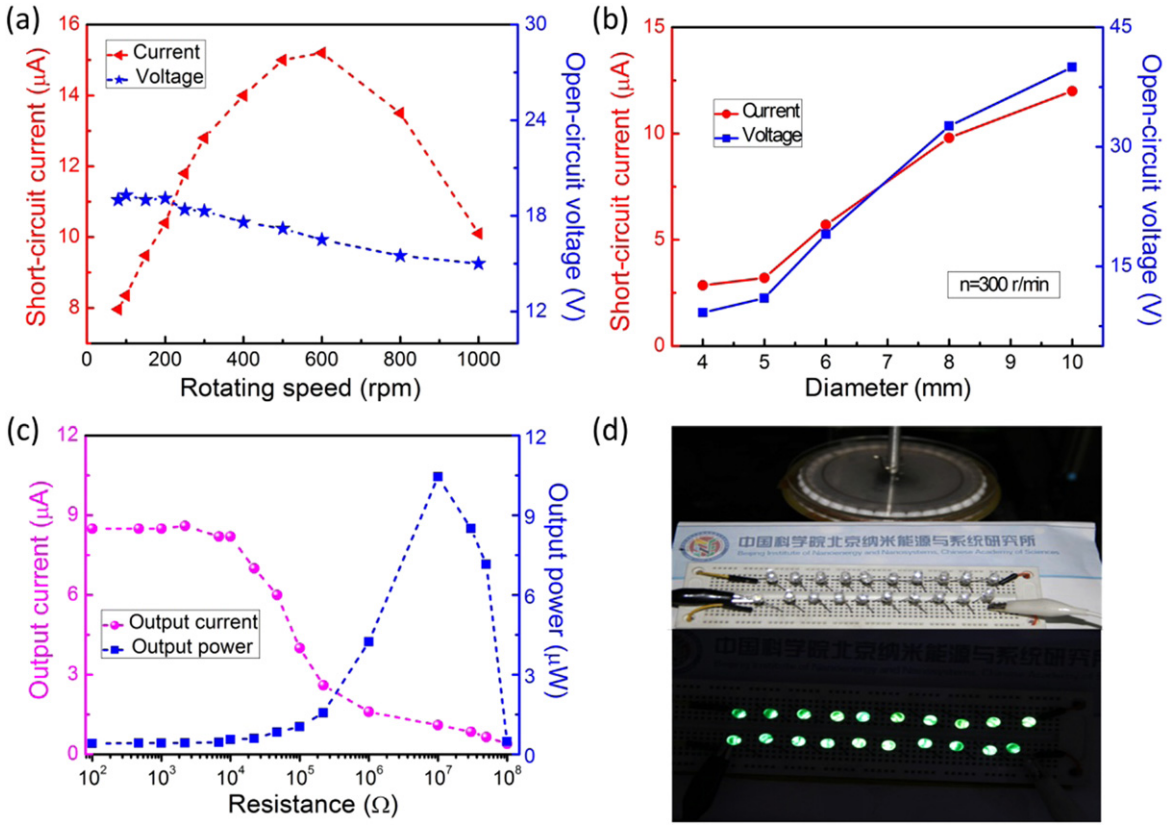

Figure 4. Electrical output characterization of the B-TENG. (a) The relationship between I_{SC}/V_{OC} and the rotating speeds. (b) The relationship between the I_{SC}/V_{OC} and the diameter of PTFE balls. (c) Dependences of the output current and output power on the external load resistance. (d) Photograph of 20 green LEDs lightened by the B-TENG.

maximum largest potential difference between electrodes A and electrodes B at the same time (as is shown in figure 3(a)). Therefore, the optimum orbit must satisfy the following relations (please see supporting information 1 available at stacks.iop.org/NANO/27/085401/mmedia):

$$D_1 = \frac{D}{\sin\theta} + D, \tag{1}$$

$$D_2 = \frac{D}{\sin\theta} - D, \tag{2}$$

$$N = \frac{360^\circ}{2\theta} = \frac{180^\circ}{\theta}, \tag{3}$$

where, D_1 is the outer diameter of the orbit, D_2 is the inner diameter of the orbit, D is the diameter of PTFE balls, N is the number of PTFE balls, which is determined by the central angle θ between the adjacent electrode A and electrode B. In the above test, the PTFE balls are 4 mm in diameter and θ is 2.5°, thus PTFE is 72 in number.

Here, we define that M is the number of the Cu interdigitative-electrodes, and the best proper orbit definitely must meet the equation $M = 2N$. Schematic diagrams of three different orbits at $M = 2N$, $M < 2N$ and $M > 2N$ are demonstrated in the figures 3(a)–(c), where the parameter θ, rather than the orbit radius of PTFE balls is changed. When $M = 2N$, the V_{OC} has cyclic outputs at a continuous amplitude of about 18 V (figure 3(d)), and I_{SC} with a constant peak of about 12 μA (figure 3(g)) is obtained. Once $M < 2N$, V_{OC} and I_{SC} outputs oscillate at a nonuniform amplitude and relevant maximum peak values decrease to ~12 V and ~8 μA (figures 3(e) and (h)), respectively. Such a change also appears when $M > 2N$, where the amplitude of V_{OC} and I_{SC} outputs become inconsistent and their maximum peaks diminish to ~14 V and ~9 μA (figures 3(f) and (i)). Those changes are mainly due to a reduced potential difference between the interdigitative-electrodes compared to the $M = 2N$ condition illustrated in the figure 2(a), which leads to a decrease in transferred charge quantity. As a result, in order to obtain the maximum output of B-TENG, the diameter of PTFE balls must match with gap between the electrodes or they should agree with that equation $M = 2N$, therefore the following tests are all operated under this condition.

To further systematically study the electric performance of B-TENG, a serials of factors that could influence the final output were tested in figure 4. The relationship between I_{SC}/V_{OC} and the rotating speed is shown in figure 4(a) (PTFE balls are 4 mm in diameter, the number of PTFE balls is 72, θ is 2.5°). The I_{SC} increases from ~8 μA to ~15 μA when the rotating speed n changes from 100 rpm to 600 rpm, and then it drops to ~10 μA as the rotating speed increases to 1000 rpm gradually. The V_{OC} remains stable when the rotating speed is no more than 200 rpm, while it will decrease with further increasing the speed to 1000 rpm. This phenomenon is likely attributed to insufficient contact between PTFE balls and Cu

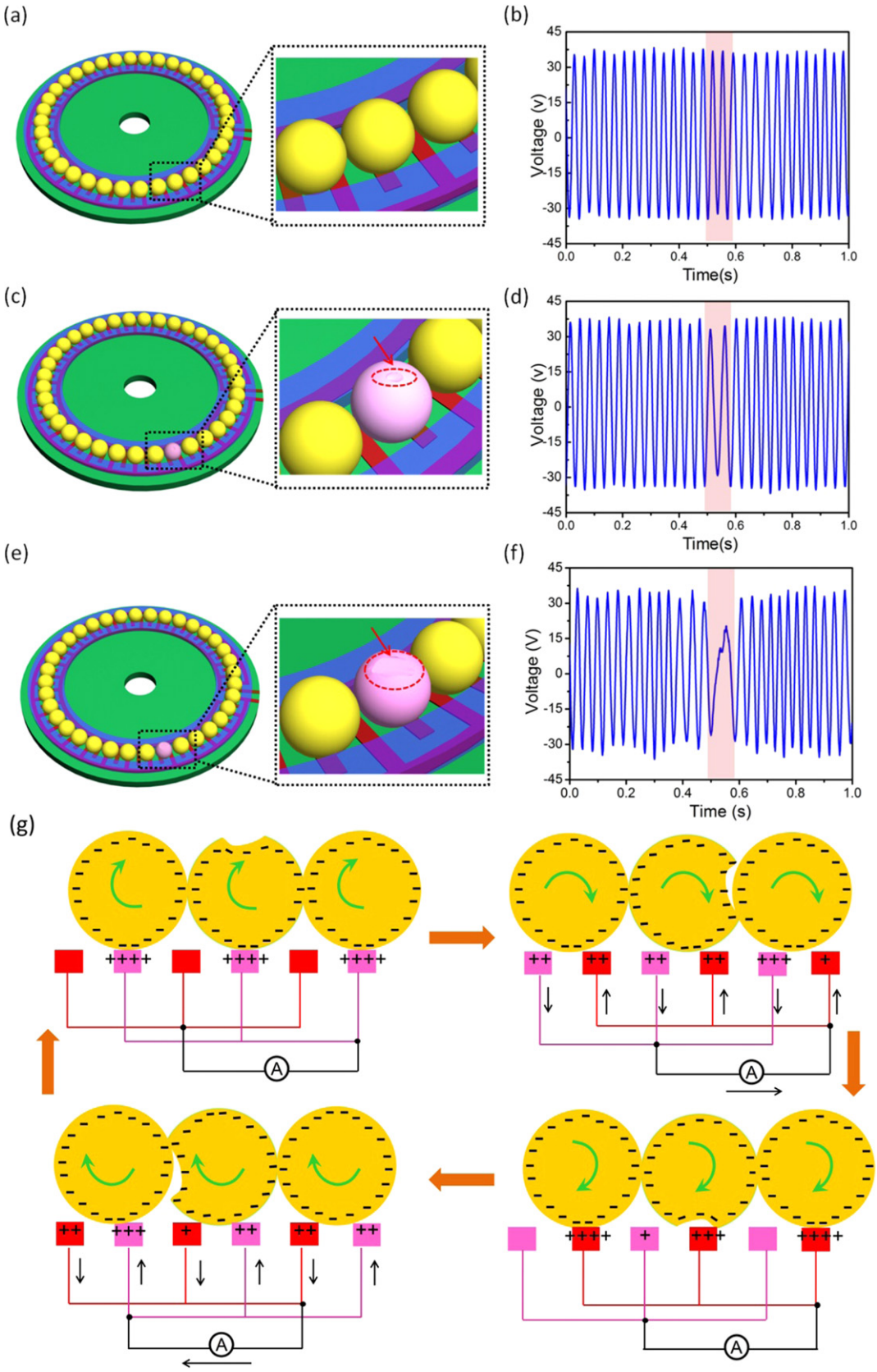

Figure 5. The damage detection of the B-TENG. (a) PTFE balls without any damage. (c) PTFE balls with a slight damage. (e) PTFE balls with a serious damage. (b) The output voltage of the B-TENG without any damage. (d) The output voltage of the B-TENG with a slight damage. (f) The output voltage of the B-TENG with a serious damage. (g) Schematic diagrams of the working principles of the B-TENG when the PTFE balls have certain damage.

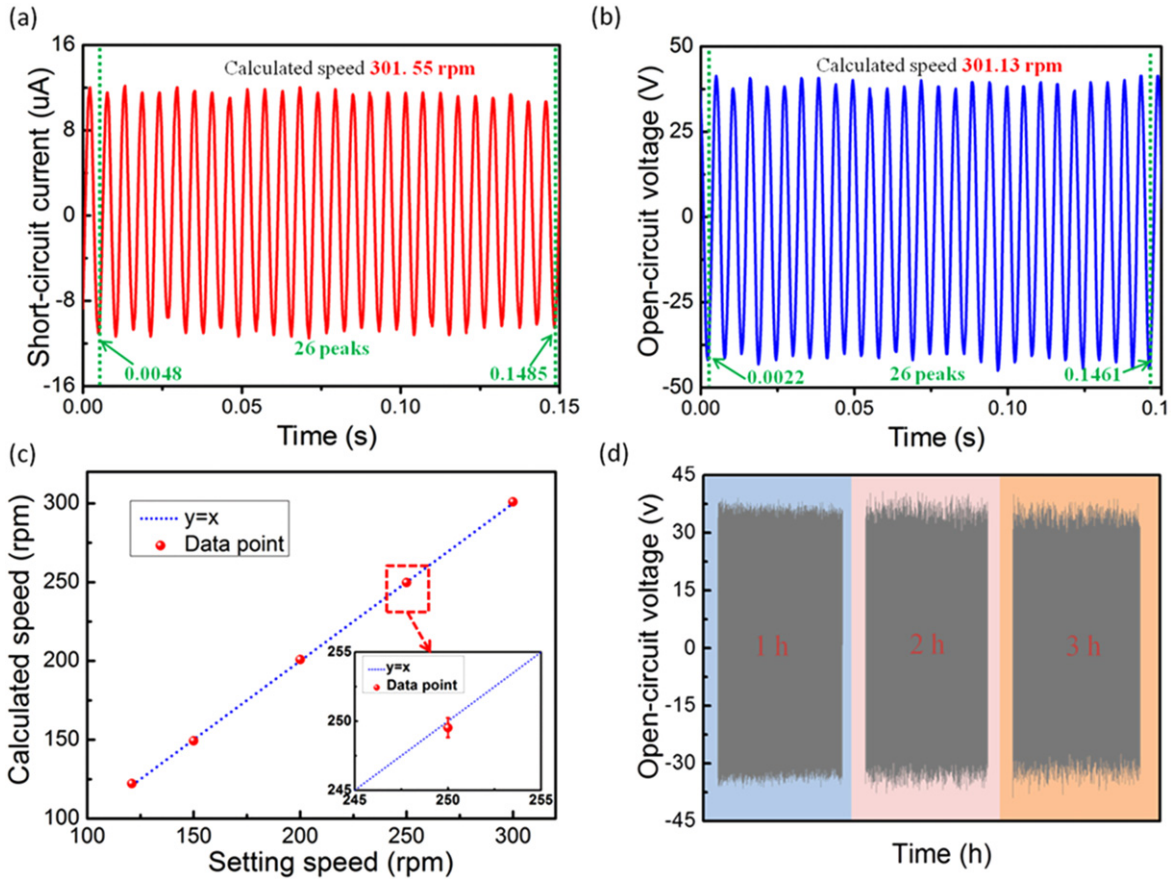

Figure 6. The rotating speed measurement of the B-TENG. (a) Randomly selected 26 current peaks at the rotating speed of 301 rpm, and the calculated speed is 301.55 rpm. (b) Randomly selected 26 voltage peaks at the rotating speed of 301 rpm, and the calculated speed is 301.13 rpm. (c) The relationship between the setting speed and the calculated speed. The inset picture is the Y error at the speed of 250 rpm. (d) Stability tests of the B-TENG for 3 h at a rotating speed of 150 rpm.

electrodes for inertia at a fairly high rotating speed, which induces the decrease of total contact charge quantity (please see supporting information S2 available at stacks.iop.org/NANO/27/085401/mmedia). In figure 4(b), different outputs were tested when the diameter of PTFE balls changed from 4 mm to 10 mm, respectively, and in this situation, the testing conditions for all the balls with 4 mm, 5 mm, 6 mm, 8 mm and 10 mm in diameter are in the same, that's θ is fixed at 5°, N is fixed at 36, and n is fixed at 300 rpm. It is obvious that both of I_{SC} and V_{OC} increase with the increasement of diameter, which is mostly due to a larger trio-surface at a larger diameter. It should be noticed that the V_{OC} and I_{SC} of the B-TENG with PTFE balls 4 mm in diameter in the figure 4(b) is not in accord with that in the figure 4(a), when the rotating speed is 300 rpm. This phenomenon is due to the change in the adjacent electrodes θ or the number of PTFE balls N. The detailed relationship between the V_{OC}/I_{SC} and θ/N is in the supporting information S3. The power output performance of the B-TENG was investigated by using different external loads (PTFE balls are 4 mm in diameter). As shown in figure 4(c), the output current gradually decreases as the resistance increases from 100 Ω to 100 MΩ. While, the output power density of the B-TENG increases in the resistance region from 100 Ω to 10 MΩ and then decreases under larger loads (>10 MΩ). As a result, the output power is maximized at 10.5 μW at the road resistance of 10 MΩ. As a power source, the B-TENG can be used to light up 20 commercial green LEDs at the same time, as shown in figure 4(d).

Application

As a crucial component in the real machine, the damage of those PTFE ball bearings may bring a negative effect on the operation of the instruments. Here, we propose a self-powered nondestructive detection sensor for monitoring the balls' damage based on the B-TENG. As depicted in figure 5, sketches in figures 5(a), (c) and (e) demonstrate the conditions that all of the balls are intact, one of the balls has a slight damage, and one of the balls has a serious damage, with their corresponding open-circuit voltage signals shown in figures 5(b), (d), and (f), respectively. Figure 5(b) depicts the cyclic signals with relatively constant amplitude of 38 V and a stable frequency when all of the bearings run well. However, some signals, oscillating at a lower frequency, show an abrupt reduction in peak value when the PTFE ball has a slight damage, as marked in figure 5(d). Such a phenomenon also occurs when a serious damage appears on the PTFE ball. In

contrast with the signals in figure 5(b), some AC outputs, highlighted in figure 5(f), have a sharp decrease in the amplitude, as well as a larger time difference or a shrinking oscillation frequency. Simultaneously, the whole signals fluctuate slightly without constant amplitude.

The reason for this phenomenon is explained in figure 5(g). When the PTFE balls roll on the disk, the damage site will contact with adjacent balls, thus leading to a shortened center-to-center distance (stage B and stage D), which is similar to the condition illustrated in figure 3(b). It is a certain situation where the PTFE ball with certain damage has inhomogeneous charge distribution on its surface, as well as the inducing positive charges unevenly distributing on the Cu electrodes, which finally causes the decline of electric potential difference between the interdigitative-electrodes, and the reduction tend to increase as the damage gets worse due to a more asymmetric charge distribution. The marks in figures 5(d) and (f) are both caused by the damage as the PTFE balls roll through the Cu electrodes.

Furthermore, the B-TENG can also serve as a self-powered rotating speed measurement sensor, based on the output electric signals. When PTFE balls (10 mm in diameter) roll on the disk at a rotating speed of 301 rpm, relevant I_{SC} and V_{OC} are illustrated in figures 6(a) and (b), respectively. Here, 26 current/voltage peaks are randomly chosen in the two figures, and corresponding rotating speed (n) are calculated by the following equation (figure S4, supporting information, available at stacks.iop.org/NANO/27/085401/mmedia):

$$n = 2 \times \frac{60k}{N(T_2 - T_1)}, \tag{4}$$

where T_2 and T_1 are the randomly selected ending time and starting time, k is the corresponding number of signal peaks between T_2 and T_1, N is number of PTFE balls. The calculated results are 301.55 rpm from current signal in figure 6(a) and 301.13 rpm from voltage signal in the figure 6(b) based on equation (4), which both fit well with the setting rotating speed of 301 rpm.

Besides, a variety of rotating speed from 120 rpm to 300 rpm were tested in figure 6(c), and the corresponding data points fall exactly on the linear curve of $y = x$, manifesting that the calculated speed fits well with the setting one. The figure insert shows an enlarged view at the data point of 250 rpm, and its error is only about 0.1% at this point. The error bar, in all figures, representing the standard deviation from repeated measurements, is less than 0.8. Furthermore, the output performance of B-TNEG is continuously tested for 3 h to demonstrate it stability in figure 6(d), and the result shows that the voltage value mainly keeps a constant during the experiment, which proves the reliability of B-TNEG as a viable method for practical applications.

Conclusion

In summary, for the first time, we proposed a self-powered and convenient nondestructive detection sensor for inspecting bearing flaws using triboelectrification. Based on the charge transfer between the Cu interdigitative-electrodes, the as-fabricated bearing-structured based triboelectric nanogenerator (B-TENG) produces an open-circuit voltage of ~40 V and a short-circuit current of ~1.2 μA at a rotating speed of 300 rpm when the PTFE balls are 4 mm in diameter. Through inspecting the produced disordered signals, the B-TENG can realize damage detection without disassembling of the whole bearing. Moreover, the B-TENG was able to monitor the rotating speed in real time by analyzing the produced cycle signals, acting as a self-powered rotating sensor. Our research presents a type of TENG for multi-functional self-powered system, which will have broad applications in fields of self-powered sensors, industrial inspection, and energy harvesting.

Acknowledgments

Thanks for the support from the 'thousands talents' program for pioneer researcher and his innovation team, China; Natural Science Foundation of Beijing, China (Grant No. 4154090), National Natural Science Foundation of China (Grant No. 51432005), the financial support by NSFC (Grant No. 61405131) and Beijing City Committee of Science and Technology (Z131100006013004, Z131100006013005). The authors declare no competing financial interest.

References

[1] Zhang J, Drinkwater B W, Wilcox P D and Hunter A J 2010 Defect detection using ultrasonic arrays: the multi-mode total focusing method *NDT&E Int.* **43** 123–33
[2] Sun T, Xu H R and Ying Y B 2009 Progress in application of near infrared spectroscopy to nondestructive on-line detection of products/food quality *Spectrosc. Spect. Anal.* **29** 122–6
[3] Kaittanis C, Santra S and Perez J M 2009 Role of nanoparticle valency in the nondestructive magnetic-relaxation-mediated detection and magnetic isolation of cells in complex media *J. Am. Chem. Soc.* **131** 12780–91
[4] Valdes S H D and Soutis C 2000 Health monitoring of composites using lamb waves generated by piezoelectric devices *Plast. Rubber Compos.* **29** 475–81
[5] Chan J W, Taylor D S, Lane S M, Zwerdling T, Tuscano J and Huser T 2008 Nondestructive identification of individual leukemia cells by laser trapping Raman spectroscopy *Anal. Chem.* **80** 2180–7
[6] Mauer L J, Chernyshova A A, Hiatt A, Deering A and Davis R 2009 Melamine detection in infant formula powder using near- and mid-infrared spectroscopy *J. Agric. Food Chem.* **57** 8062
[7] Diamanti K and Soutis C 2010 Structural health monitoring techniques for aircraft composite structures *Prog. Aerosp. Sci.* **46** 342–52
[8] Schoen R R, Habetler T G, Kamran F and Bartheld R G 1995 Motor bearing damage detection using stator current monitoring *IEEE Trans. Ind. Appl.* **31** 1274–9
[9] Wang Z L 2014 Triboelectric nanogenerators as new energy technology and self-powered sensors-principles, problems and perspectives *Faraday Discuss.* **176** 447–58

[10] Wang S H, Lin L and Wang Z L 2015 Triboelectric nanogenerators as self-powered active sensors *Nano Energy* **11** 436–62
[11] Fan F R, Tian Z Q and Wang Z L 2012 Flexible triboelectric generator! *Nano Energy* **1** 328–34
[12] Han C B, Du W M, Zhang C, Tang W, Zhang L M and Wang Z L 2014 Harvesting energy from automobile brake in contact and non-contact mode by conjunction of triboelectrication and electrostatic-induction processes *Nano Energy* **6** 59–65
[13] Chen J, Zhu G, Yang J, Jing Q, Bai P, Yang W, Qi X, Su Y and Wang Z L 2015 Personalized keystroke dynamics for self-powered human–machine interfacing *ACS Nano* **9** 105–16
[14] Zhu G, Yang W Q, Zhang T J, Jing Q S, Chen J, Zhou Y S, Bai P and Wang Z L 2014 Self-powered, ultrasensitive, flexible tactile sensors based on contact electrification *Nano Lett.* **14** 3208–13
[15] Yang Y, Zhang H L, Lin Z H, Zhou Y S, Jing Q S, Su Y J, Yang J, Chen J, Hu C G and Wang Z L 2013 Human skin based triboelectric nanogenerators for harvesting biomechanical energy and as self-powered active tactile sensor system *ACS Nano* **7** 9213–22
[16] Yang P K, Lin L, Yi F, Li X, Pradel K C, Zi Y, Wu C I, He J H, Zhang Y and Wang Z L 2015 A Flexible, stretchable and shape-adaptive approach for fersatile energy conversion and self-powered biomedical monitoring *Adv. Mater.* **27** 3817–24
[17] Tang W, Zhou T, Zhang C, Fan F R, Han C B and Wang Z L 2014 A power-transformed-and-managed triboelectric nanogenerator and its applications in a self-powered wireless sensing mode *Nanotechnology* **25** 225402
[18] Tang W, Meng B and Zhang H X 2013 Investigation of power generation based on stacked triboelectric nanogenerator *Nano Energy* **2** 1164–71
[19] Wen X N, Yang W Q, Jing Q S and Wang Z L 2014 Harvesting broadband kinetic impact energy from mechanical triggering/vibration and water waves *ACS Nano* **8** 7405–12
[20] Chen J, Zhu G, Yang W Q, Jing Q S, Bai P, Yang Y, Hou T C and Wang Z L 2013 Harmonic-resonator-based triboelectric nanogenerator as a sustainable power source and a self-powered active vibration sensor *Adv. Mater.* **25** 6094–9
[21] Meng X S, Li H Y, Zhu G and Wang Z L 2015 Fully enclosed bearing-structured self-powered rotation sensor based on electrification at rolling interfaces for multi-tasking motion measurement *Nano Energy* **12** 606–11
[22] Han C B, Zhang C, Li X H, Zhang L M, Zhou T, Hu W G and Wang Z L 2014 Self-powered velocity and trajectory tracking sensor array made of planar triboelectric nanogenerator pixels *Nano Energy* **9** 325–33
[23] Wu Y, Jing Q S, Chen J, Bai P, Bai J J, Zhu G, Su Y J and Wang Z L 2015 A self-powered angle measurement sensor based on triboelectric nanogenerator *Adv. Funct. Mater.* **25** 2166–74
[24] Han C B, Zhang C, Tang W, Li X H and Wang Z L 2015 High power triboelectric nanogenerator based on printed circuit board (PCB) technology *Nano Res.* **8** 722–30